EUROPEAN ORGANIZATION FOR NUCLEAR RESEARCH

CERN-EP/88-109
30 August 1988

A-DEPENDENCE OF LOW-MASS MUON PAIR PRODUCTION IN 300 GeV/c p AND 320 GeV/c π^- INTERACTIONS

WA 78 Collaboration

H. Cobbaert and R. Roosen
Inter-University Institute for High Energies, ULB-VUB, Brussels, Belgium

M.G. Catanesi, M.T. Muciaccia, S. Natali, S. Nuzzo and F. Ruggieri
Università di Bari and INFN, Bari, Italy

G. Carboni[1], G. Crosetti[2], M. Fidecaro, C. Gerke[3], G. Poulard and H. Sletten
CERN, Geneva, Switzerland

M. Coupland, I.G. Roberts and P.T. Trent
Birkbeck College, London, UK

J.H. Bartley, J.E. Conboy, M.J. Esten, P. Fennel and P.F. Harrison
University College London, UK

M. De Vincenzi, S. Di Liberto, A. Frenkel, M. Iori, E. Lamanna, G. Marini[4], G. Martellotti, F. Meddi, A. Nigro, G. Penso, S. Petrera, P. Pistilli[5], G. Romano[4], G. Rosa and A. Sciubba
Università di Roma 'La Sapienza' and INFN, Rome, Italy

B. Alessandro, V. Bisi, D. Gamba, L. Ramello and L. Riccati
Università di Torino and INFN, Turin, Italy

(Submitted to Physics Letters B)

Present addresses:
1) INFN, Pisa, Italy.
2) INFN, Genoa, Italy.
3) DESY, Hamburg, Fed. Rep. Germany.
4) Università di Salerno and INFN, Salerno, Italy.
5) Università di Lecce and INFN, Lecce, Italy.

ABSTRACT

The A-dependence of inclusive $\mu^+\mu^-$ production is measured in the kinematical region $2m_\mu \leqslant m(\mu^+\mu^-) \lesssim 1.5$ GeV/c^2, $0.1 \lesssim x_F(\mu^+\mu^-) \lesssim 0.6$, using a 300 GeV/c p beam and a 320 GeV/c π^- beam, on Al, Fe, and U targets. Assuming that the production cross-section varies as A^α, we obtain $\alpha = 0.68 \pm 0.03^{+0.02}_{-0.05}$ for the p beam and $\alpha = 0.80 \pm 0.02^{+0.02}_{-0.05}$ for the π^- beam.

We present an experimental comparison of the inclusive low-mass $\mu^+\mu^-$ production cross-section, measured at the CERN Super Proton Synchrotron (SPS) with 300 GeV/c proton and 320 GeV/c negative pion beams on three different materials: Al, Fe, and U.

The apparatus, which has been described in detail elsewhere [1], consists essentially of a variable-density target calorimeter followed by a muon spectrometer, equipped with drift and multiwire proportional chambers and a superconducting magnet (1.5 T). This enables us to measure the muon momentum with a resolution of $\Delta p/p = 6 \times 10^{-4}\, p(GeV/c)$.

The target calorimeter is divided into 25 modules. Each module consists of four absorber plates interleaved with four sheets of 5 mm thick plastic scintillator. Light signals from the four scintillators of a module are conveyed through optical fibres to a single photomultiplier. The first 13 (upstream) modules form the target section, which is expandable and allows an easy change of the absorbers and of their density. The remaining 12 (downstream) modules, with iron absorbers, are kept fixed. All modules of the target section contain absorbers of the same material for the Fe and the U runs, but in the case of Al, owing to its longer interaction length, only the first five modules of the target section contain Al absorbers, whilst the last eight modules contain U. The different configurations of the calorimeter are reported in table 1.

The muon trigger and off-line selection criteria have been already described in detail for p [2] and π^- [3] runs. Events are required to have at least one muon reconstructed in the spectrometer, with a momentum in the interval $20 \leqslant p_\mu \leqslant 100$ GeV/c and the energy deposited in the calorimeter between 80 and 400 GeV. These conditions ensure a good spectrometer reconstruction and eliminate beam-muons, halo-muons, and pile-up effects due to two coincident beam particles in the calorimeter.

For each material, data have been taken at three different densities ϱ of the target section of the calorimeter, namely $1/\varrho = 1$ (compact form), 1.5, and 2. It was shown in refs. [2] and [3] that the dimuon rate is independent of the target density as expected for a prompt process. In the present analysis, we have used only the data taken with the calorimeter in compact form ($\varrho = 1$). The statistics accumulated in this configuration are sufficiently high to give comparable statistical and systematic errors.

Table 2 lists the number of effective interactions collected with Al, Fe, and U targets and with p and π^- beams.

Figure 1 shows the μ^+ and μ^- momentum distributions and the dimuon Feynman x distribution for different target materials and beam particles. All these distributions have been normalized to the same integral. We observe that the μ^+ and the μ^- momentum distributions corresponding to the same beam particle are almost identical, as expected for electromagnetic processes. The momentum and x_F distributions corresponding to different materials are also quite similar, showing that these quantities are scarcely affected by nuclear effects. However, the muons produced in π^- interactions are, on the average, more energetic than those coming from p interactions. This is expected if we consider the difference in π^- and p structure functions, and is in agreement with what was found in ref. [4].

Also shown in fig. 1 are the predictions of a Monte Carlo calculation, normalized to the experimental points. These predictions have been calculated using the parametrization of the low-mass dimuon production cross-section given in ref. [4]. The production of muon pairs by secondary particles (hadrons and photons) interacting in the calorimeter was also taken into account. This contribution is of the order of 20% of the total number of observed dimuons. It has been evaluated assuming an inclusive longitudinal differential cross-section for the secondary particles as given in ref. [5], and taking into account the A-dependence of the inclusive x_F distribution as reported in ref. [6]. The contribution from charm decay was estimated to be of the order of 5% of the observed dimuons, using the prompt single-muon rate measured in our experiment [2, 3]. The

final prediction of the Monte Carlo is nearly independent of the target material, so only one histogram is plotted in fig. 1 for each distribution. We find the predictions are in quite good agreement with the experimental data.

Figure 2 shows the dimuon mass distribution for different target materials and beam particles. The histograms are Monte Carlo predictions, calculated as in fig. 1. Although the muon momentum distributions for each material were similar, the dimuon mass distributions are different. This is due to the multiple scattering in the calorimeter dump, which causes a shift of 50–100 MeV/c^2 toward higher mass values and also a spread of 150–200 MeV/c^2 (r.m.s.). This effect is particularly evident for the U target. Note that owing to the presence of U in the Al target section (see table 1), the effect on the Al data is intermediate between that of Fe and U. Therefore the acceptance of the set-up, at a fixed dimuon mass, depends on the material. However, this dependence becomes negligible when integrated over the mass region between threshold and 1.5 GeV/c^2, so we shall not give the A-dependence as a function of the measured dimuon mass, but only of x_F, which is insensitive to multiple scattering.

The experiment accepts dimuons with $0.1 \lesssim x_F \lesssim 0.6$, these limits being almost independent of the dimuon mass, as shown in fig. 3.

In table 3 and fig. 4a we report the dimuon rate for the Al, Fe, and U targets, and for the p and π^- beams. Parametrizing the muon pair production cross-section in the accepted kinematical region as $\sigma \propto A^\alpha$, the fitted slopes of fig. 4a, combined with the A-dependence of the total absorption cross-section [7], lead to the following results:

$$\alpha = 0.68 \pm 0.03 \,^{+0.02}_{-0.05} \qquad \text{for the p beam ,}$$

$$\alpha = 0.80 \pm 0.02 \,^{+0.02}_{-0.05} \qquad \text{for the } \pi^- \text{ beam .}$$

The second (systematic) errors were evaluated taking into account the contamination from non-prompt and beam muons, and the failure of the pattern recognition software to resolve two muon tracks produced with a very small opening angle. This effect is partly compensated by multiple scattering, which — especially for denser material — reduces the number of unresolved pairs.

Finally, fig. 4b shows the values of α measured in different x_F intervals. Our results are compatible with the behaviour of α versus x_F observed in other experiments [8] for low dimuon mass.

In conclusion, we have measured the A-dependence of inclusive muon pair production for dimuon masses between threshold and 1.5 GeV/c^2 and $0.1 \lesssim x_F \lesssim 0.6$. Our results confirm that for low dimuon masses, α is significantly lower than 1, and extend the measurements performed in previous experiments [8] down to dimuon threshold.

REFERENCES

[1] M.G. Catanesi et al., Nucl. Instrum. Methods **A253** (1987) 222.

[2] H. Cobbaert et al., Phys. Lett. **206B** (1988) 546.

[3] H. Cobbaert et al., Phys. Lett. **191B** (1987) 456.

[4] K.J. Anderson et al., Phys. Rev. Lett. **37** (1976) 799 and 803. For the π^- beam we have used the data relative to the π^+ beam reported in this reference.

[5] M. Adamus et al., Charged-particle production in K^+p, π^+p, and pp interactions at 250 GeV/c, to be published in Z. Phys. C.
M. Aguilar-Benitez et al., Europhys. Lett. **4** (1987) 1261.

[6] D.S. Barton et al., Phys. Rev. **D27** (1983) 2580.

[7] A.S. Carroll et al., Phys. Lett. **80B** (1979) 319. Following this reference we have taken for the total absorption cross-section of p and π^- on nuclei, $\sigma_{abs} \propto A^{0.72}$ and $A^{0.75}$, respectively.

[8] M. Binkley et al., Phys. Rev. Lett. **37** (1976) 571.
J.G. Branson et al., Phys. Rev. Lett. **38** (1977) 1334.
K.J. Anderson et al., Phys. Rev. Lett. **42** (1979) 944.
R. Bailey et al., Z. Phys. **C22** (1984) 125.

Table 1

Summary of calorimeter configurations

Al target	Fe target	U target	
50 mm Al	25 mm Fe	10 mm U	Expandable
(× 20)	(× 52)	(× 20)	
15 mm U		15 mm U	Expandable
(× 32)		(× 32)	
25 mm Fe	25 mm Fe	25 mm Fe	Fixed
(× 48)	(× 48)	(× 48)	

Table 2

Total effective number of interactions for the three targets

Target	p beam	π^- beam
Al	1.3×10^7	2.7×10^7
Fe	8.6×10^7	1.3×10^7
U	7.6×10^7	7.7×10^7

Table 3

Number of dimuon events per 10^6 effective interactions

Target	p beam	π^- beam
Al	14.7 ± 1.1	32.7 ± 1.0
Fe	13.1 ± 0.4	31.3 ± 1.6
U	12.7 ± 0.4	36.1 ± 0.7

Figure captions

Fig. 1 : Normalized distribution of μ^+ and μ^- momentum and Feynman x of the muon pair, for different target materials and beam particles. The upper (lower) figures refer to the p (π^-) beam. For the sake of clarity, triplets of points relative to Al, Fe, and U have been drawn separately but refer to the same bin of p^+, p^-, or x_F. Histograms are Monte Carlo predictions calculated as explained in the text.

Fig. 2 : Normalized distribution of muon-pair mass, for different target materials and beam particles. Histograms are Monte Carlo predictions calculated as explained in the text.

Fig. 3 : Acceptance of the experiment versus the x_F of the dimuon, for two values of the dimuon mass.

Fig. 4 : a) Dimuon rate versus atomic number of the target, for the p and π^- beams. The full line is an A^α fit to the three points. The dashed line shows the slope for an A^1 dependence. b) α versus x_F. The errors on α are statistical only.

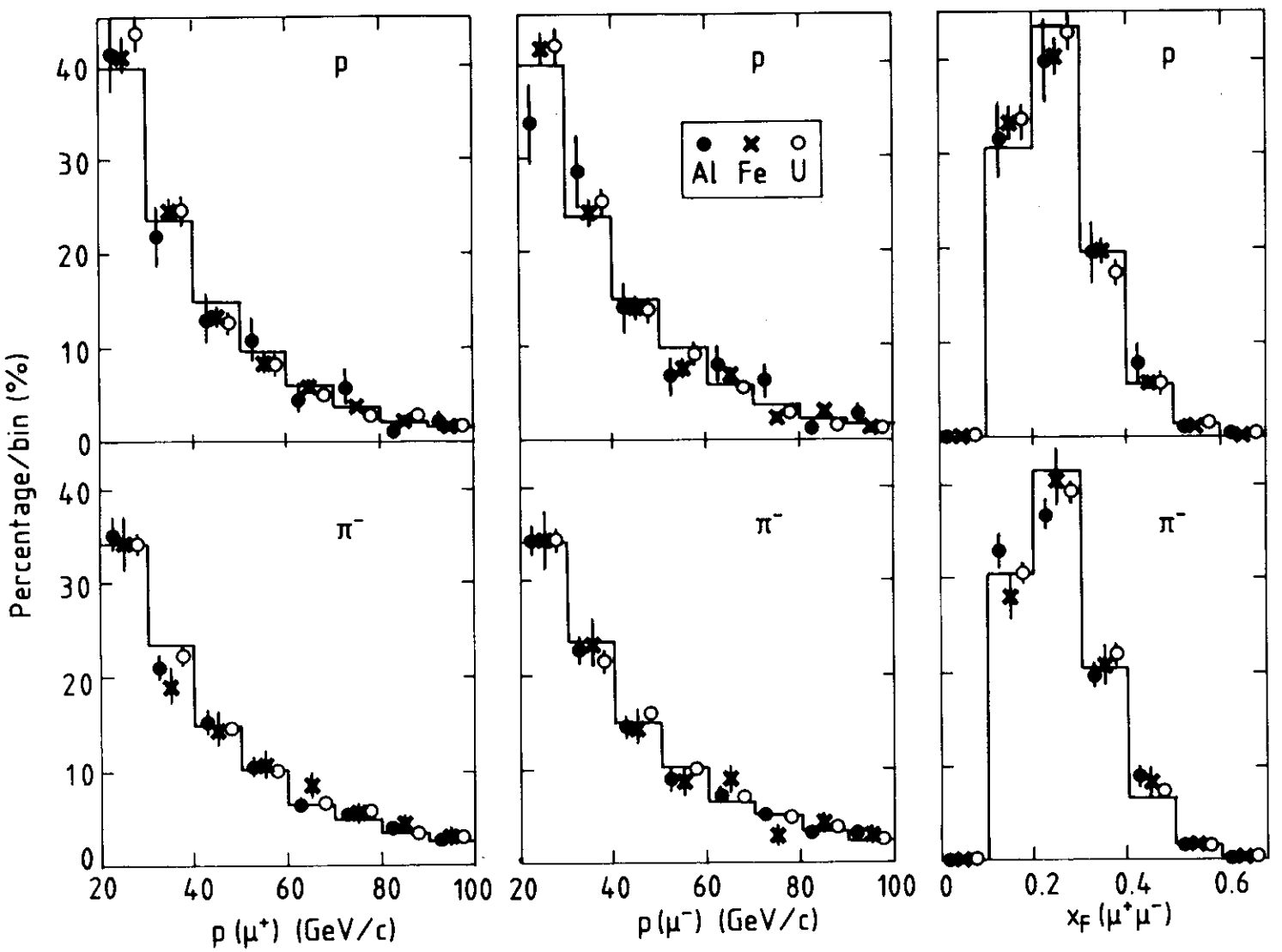

Fig. 1

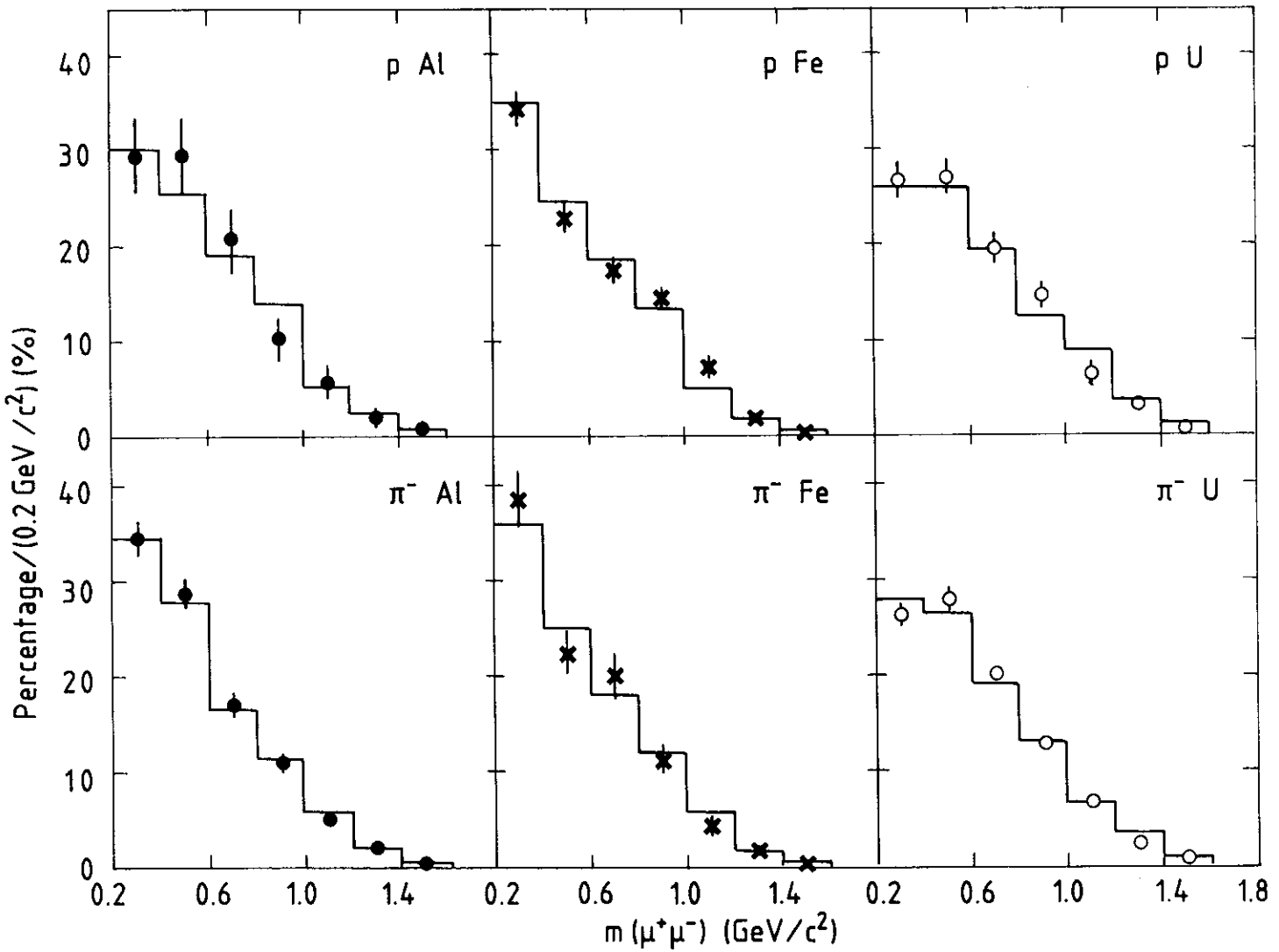
p Al
p Fe
p U
π⁻ Al
π⁻ Fe
π⁻ U
Percentage/(0.2 GeV/c²) (%)
m (μ⁺μ⁻) (GeV/c²)
0
10
20
30
40
0.2
0.6
1.0
1.4
1.8

Fig. 2

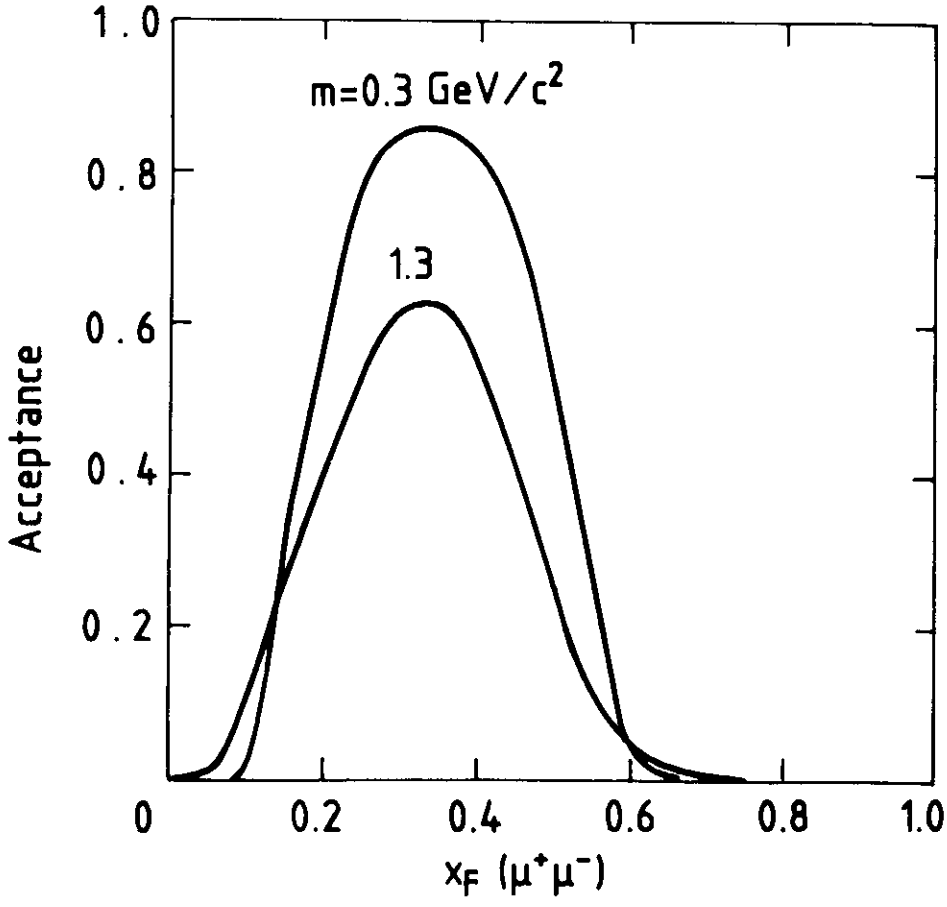

Fig. 3

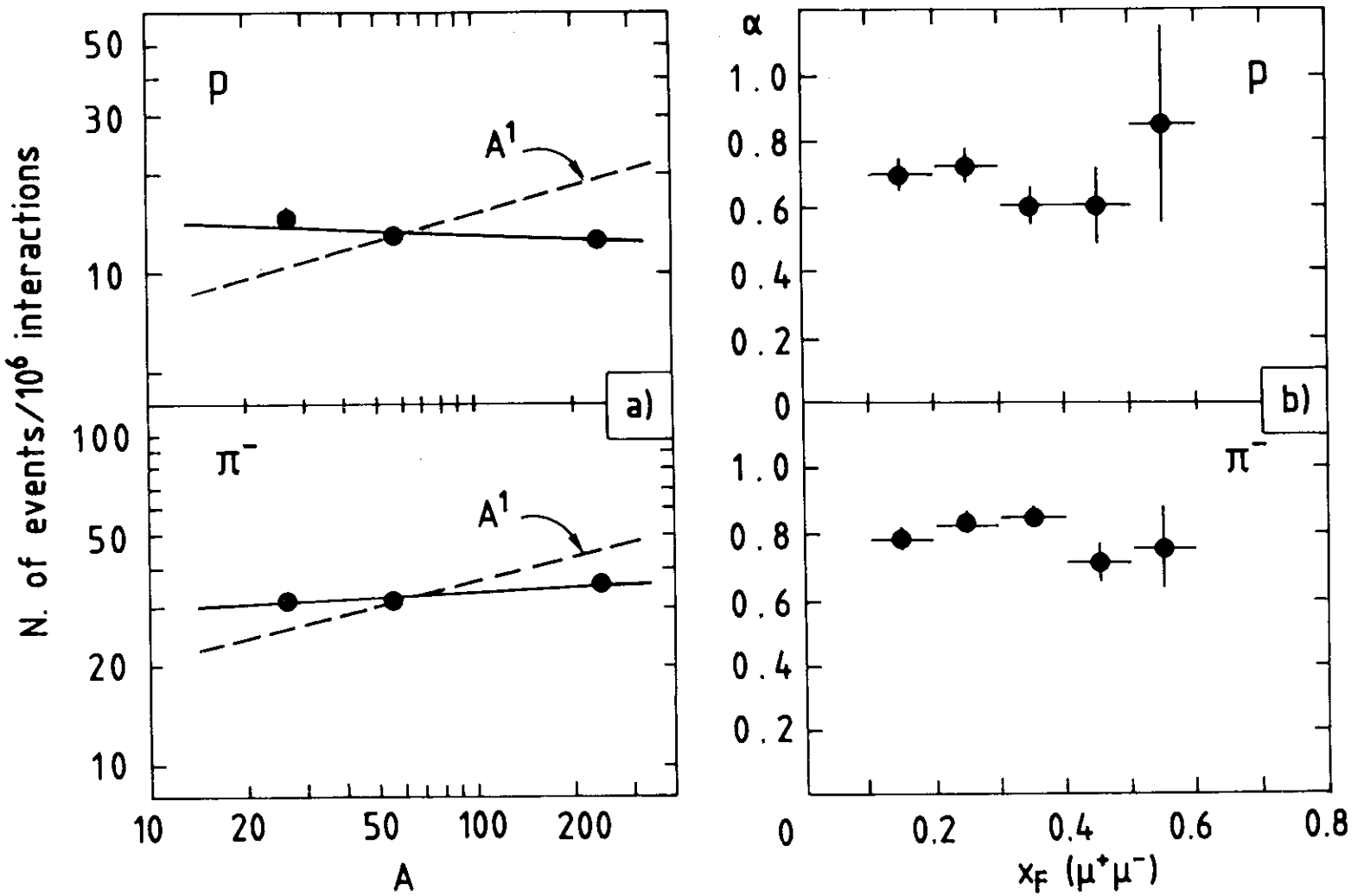
N. of events/10^6 interactions
p
A^1
a)
π⁻
A^1
50
30
10
100
50
20
10
10
20
50
100
200
A
α
p
1.0
0.8
0.6
0.4
0.2
0
b)
π⁻
1.0
0.8
0.6
0.4
0.2
0
0.2
0.4
0.6
0.8
x_F (μ⁺μ⁻)

Fig. 4